Combinatorial Preparation and Characterization Methods for High Throughput Study of Advanced Functional Materials

Closing report

Principal investigator: Fried, Miklós (MTA Centre for Energy Research, Institute of Technical Physics and Materials Science) Participants: Zolnai, Zsolt, Lábadi, Zoltán, Lohner, Tivadar, Serényi, Miklós, Sáfrán, György, Cora, Ildikó, Kovács Kis, Viktória (researchers) Jakab, Andrea, Lázár, Csaba, Szász, Noémi

NKFI-ID: 129009 Type: K

Project Summary (*from the original Application*) The physical, chemical and structural properties of the cutting-edge materials are strongly dependent on their composition. The common procedure to reveal the properties of concentration dependent phases is the preparation of numerous two (or more)-component samples, one for each C(a)/C(b=1-a) composition, and the investigation of these individuals. This is a low efficiency procedure that costs enormous time of man and machine. Contrarily, using the combinatorial material synthesis approach, materials libraries can be produced in one experiment that contain up to several hundreds or thousands of samples on a single substrate. In order to identify optimized material structures in an efficient way, adequate automated micro-spot material characterization tools have to be applied. The preparation devices (DC magnetron, pulsed mode reactive DC magnetron and biased RF sputtering systems as well as laser ablation deposition system) and characterization instruments (SE-Spectroscopic Ellipsometry, RBS-Rutherford Backscattering Spectrometry, TEM-Transmission Electron Microscopy, SEM-Scanning Electron Microscopy, AFM-Atomic Force Microscopy) which can be used in MFA offer powerful tools for the fabrication and processing of materials libraries as well as for accelerated material characterization on appropriate planar substrates such as Si or oxidized Si wafers. These methods can help us to search more efficient advanced functional materials for micro-, nano- and optoelectronics, energy converters (solar cells) or different (optical or gas) sensor systems.

Sample preparation

We optimized the (RF and DC) magnetron sputtering systems to use them for combinatorial material synthesis. As further development of our single-sample microcombinatorial method the first version of a computer-controlled power regulator for the DC magnetron sputter deposition has been worked out that replaced the former manual regulation, see Fig. 1. (See G. Sáfrán, et al: „*One-sample concept" micro-combinatory; a new approach for high throughput characterization of binary films*, Oral presentation (invited), International Conference on Material Science and Nanotechnology (ICMSN 2019), Paris, France, September 17-18, 2019; G. Sáfrán, et al: *Single sample combinatory for high throughput TEM, RBS, XRD, nanoindentation and ellipsometry studies of binary films*, Oral presentation (invited), 26th Assembly of Advanced Materials Congress (AMC), Stockholm Sweden, 10-13 June 2019; G. Sáfrán, et al: *A micro-combinatorial approach for a reveal of composition dependent properties of binary films by TEM and further analytical techniques*, Oral presentation (invited), 6th_International Congress on Microscopy and Spectroscopy Oludeniz, Turkey, May 12-18, 2019)

a-$Si_{1-x}Ge_x$:H system

We prepared Si_xGe_{1-x} sample (see Fig. 1 and G. Sáfrán, et al; „*Determination of the optical properties of a-Si_xGe_{1-x} facilitated by micro-combinatory*"; AIP Conference Proceedings, Volume 2186, Issue 1, id.170027 Pub Date: December 2019, DOI: 10.1063/1.5138106) with different hydrogen content using the single-sample micro-combinatorial technique which enables the preparation of a-$Si_{1-x}Ge_x$:H with full range composition spread. The samples were investigated by Spectroscopic Ellipsometry (SE), Rutherford Backscattering Spectrometry (RBS)- Elastic Recoil Detection Analysis (RBS-ERDA) and Transmission Electron Microscopy (TEM). The optical parameters of hydrogenated amorphous a-$Si_{1-x}Ge_x$:H layers were measured with focused beam mapping ellipsometry for photon energies from 0.7 to 6.5 eV. Linearly variable composition profile was revealed along the 20 mm long gradient part of the sample by Rutherford backscattering spectrometry and elastic recoil detection analysis. The Cody-Lorentz approach was identified as the best model to describe the dispersion of the alloy. The effect of incorporated hydrogen on the optical absorption is explained by the lowering of the density of localized states in the mobility gap. It is shown that in the low-dispersion near infrared range the refractive index of the SiGe alloy can be comprehended as a

linear combination of the optical parameters of the components. The micro-combinatorial sample preparation with mapping ellipsometry is not only suitable for the fabrication of samples with controlled lateral distribution of the concentrations, but also opens new prospects in creating databases of compounds for optical and optoelectonic applications, see Fig. 2. [B. Kalas, et al; *Micro-combinatorial sampling of the optical properties of hydrogenated amorphous $Si_{1-x}Ge_x$ for the entire range of compositions towards a database for optoelectronics*" SCIENTIFIC REPORTS 10:1 Paper: 19266 , 19 p. (2020); Lohner, T, et al; *Determination of the Complex Dielectric Function of Ion-Implanted Amorphous Germanium by Spectroscopic Ellipsometry*, *Coatings* 2020, *10*(5), 480; https://doi.org/10.3390/coatings10050480; G. Sáfrán, et al: *Determination of the optical properties of a-SixGe1-x facilitated by microcombinatory*, Poster and Proceedings, 15TH INTERNATIONAL CONFERENCE OF COMPUTATIONAL METHODS IN SCIENCES AND ENGINEERING, Rhodes, Greece May 1-5 2019.]

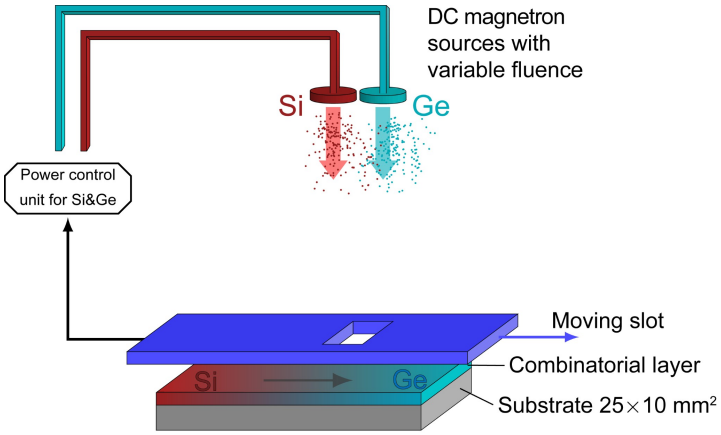

Fig 1 Setup used for the "single-sample concept" combinatorial deposition of the a-$Si_{1-x}Ge_x$:H layers.

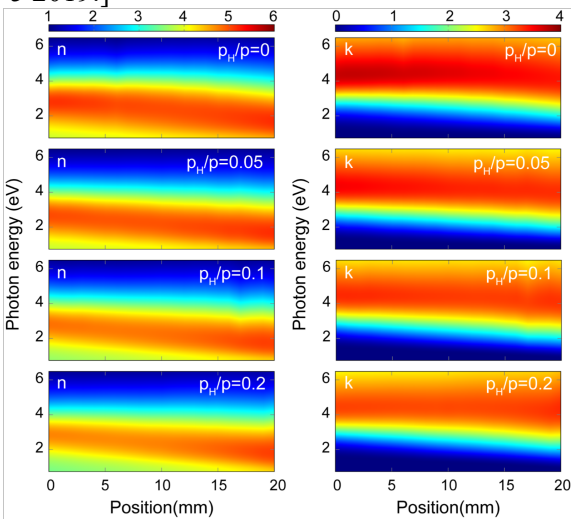

Fig 2 Real and imaginary parts of the complex refractive indices of a-$Si_{1-x}Ge_x$:H thin films (left and right column, respectively) with different partial pressures of H (p_H/p = 0,0.05, 0.1 and 0.2) as a function of both the lateral position along the 20 mm long gradient section and photon energy. In accordance with the RBS plots, the zero position corresponds to the Si-rich side of the sample.

$Si_{1-x}Ge_x$ system

Our aim was to study effectively by TEM the pair-correlation properties ie. average distances of adjacent atoms of a-Si-Ge as a function of Ge concentration in amorphous $Si_{1-x}Ge_x$ layers at the entire composition range. [I. Cora, et al, *Concentration dependent pair-correlation in amorphous $Si_{1-x}Ge_x$ layers revealed by micro-combinatorial TEM,* In: Miklós Fried (ed.) Proceedings of Anyagtudományi Szimpózium, Budapest, Magyarország: Óbudai Egyetem (2020) 44 p. pp. 26-30.]

We applied micro-combinatory based on the "one-sample concept" in which a gradient sample was prepared and studied in a single TEM grid representing a whole binary system A_xB_{1-x} (x=0...1). Thanks to all-in-one feature of the μ-combinatorial TEM specimen no need for laborious preparation, replacement and study of a series individual samples. Beside effectivity a specific advantage of μ-combinatory is that various compositions are formed and investigated side by side, within a single TEM grid that provides superior reproducibility and direct comparison for EDS and SAED measurements.

8 nm thick Si-Ge composition spread samples have been deposited by dual DC magnetron sputtering onto Czochralsky-grown NaCl single crystals in a stainless steel UHV vacuum system of $3x10^{-8}$ mbar base pressure. After removal from the vacuum system the samples were wet-stripped from the NaCl and placed on Cu TEM grids with rectangular mesh so that the gradient line was oriented diagonally to the grid bars. This assured that none of the compositions were masked out by the grid bars. The combinatorial layer track was 1 mm wide and 2.5 mm long that fits to the view field of the TEM, see Fig. 3a.

During TEM measurements a series of selected area electron diffraction (SAED) patterns were recorded with carefully controlled and reproduced camera length and lens currents along the gradient film representing various Si-Ge compositions. The local composition was determined with energy Dispersive Electron Spectrometry (EDS) by a Bruker Si-drift detector system, see Fig. 3b. The intensity distribution of

SAED-s were determined with help of the software "ProcessDiffraction" and the nearest atomic distances in the amorphous Si-Ge were calculated and plotted as a function of the elemental composition

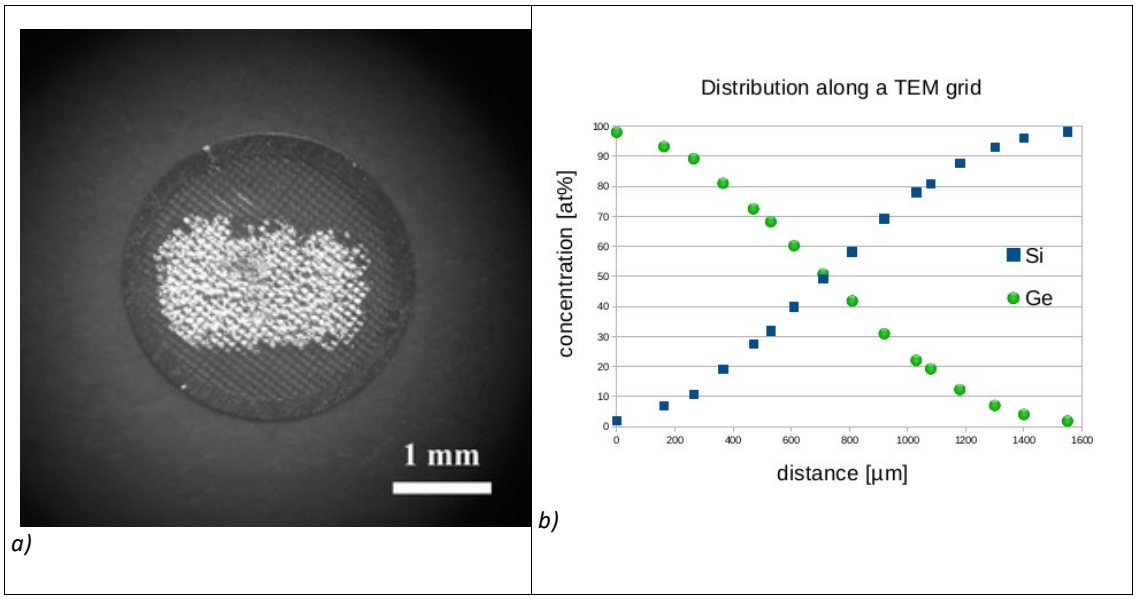

Fig.3. (a) Overview of an ultrathin (8 nm) concentration-spread µ-combinatorial SiGe sample deposited on Mo TEM grid. The 1x2 mm² sized layer consists of a 1000 µm long concentration gradient Si-Ge track enclosed by 250 µm long tracks of pure Si and Ge. (b) Concentration distribution revealed by EDS along a horizontal scan of the µ-combinatorial TEM specimen shown in (a).

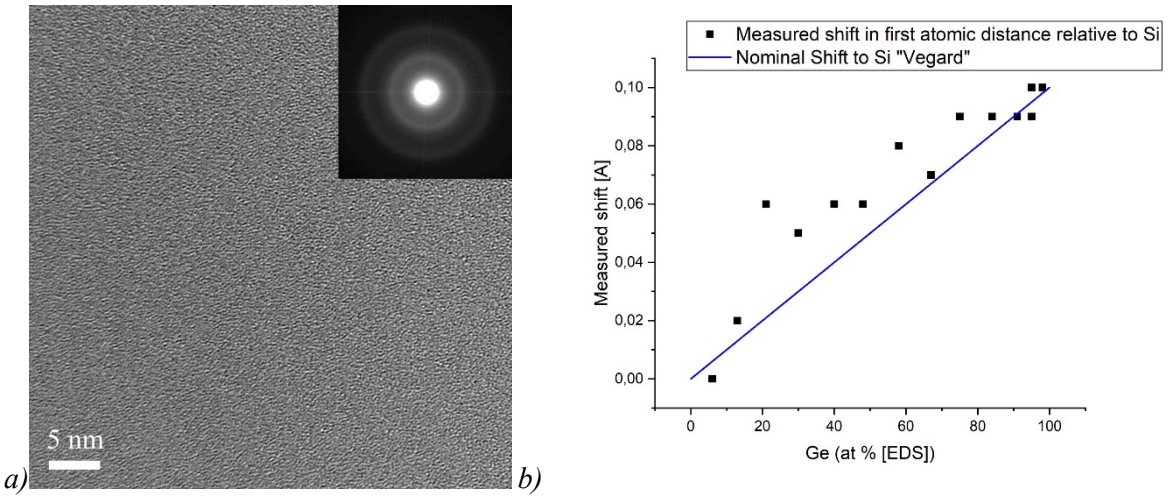

Figure 4 a) TEM micrograph with SAED inset of the ultrathin 8 nm self-supporting micro-combinatorial amorphous SiGe sample at 50/50 at% composition. b) Deviations of adjacent atomic distances from that of Si in an 8 nm thick µ-combinatorial a-SiGe sample, as a function of Ge concentration: determined from SAED measurements (square) and calculated according to the Vegard's rule (solid line).

Fig. 4 a shows a bright field TEM with a SAED inset at 50/50 at% SiGe composition of the concentration spread sample. Both TEM and SAED represent amorphous structure that was found at all compositions of the sample.

Both crystalline Si and Ge form fcc diamond structure with lattice parameters, Si: 0.5392 nm, Ge: 0.5657 nm. Applying Vegard's rule ($a(Si_{1-x}Ge_x) = (1-x)\, a(Si) + x\, a(Ge)$) we calculated the atomic distances (a) of the nearest neighbours in a-Si-Ge as a dependence of Ge concentration. These theoretical atomic distances are represented by the solid line in Fig. 4 b. Deviations from adjacent atomic distances, determined from SAED measurements of the sample of varying composition, from Si are indicated in the same diagram by squares. It is clearly seen, that the squares at the ends of the gradient range (pure Si and pure Ge) show very good fit to the calculated Vegard line, while in the gradient range (mixed compositions) they typically fall above the Vegard line. The measured values, therefore, are "forward" compared to what is calculated - that is, they show an atomic distance corresponding to a higher Ge concentration.

The average adjacent atomic distances were revealed in the entire composition range as a function of Si-Ge composition. They follow the Vegard's rule in the trend, but due to selective oxidation of Si, the diagram advances towards the values characteristic of Ge-rich compositions.

a-Si:H system

Incorporated hydrogen and its bonding configuration have an effect on the electrical and structural properties of hydrogenated amorphous silicon (a-Si:H) thin films. On one hand hydrogenization is known to be very efficient in reducing the density of dangling bonds responsible for deep levels in the bandgap; the technological process that carries out the incorporation of hydrogen improves the device parameters. On the other hand, the H–Si–H bonding configuration may negatively affect the microstructure of the amorphous lattice and promote the creation of voids.

We interpreted the incorporation of hydrogen into radio frequency sputtered amorphous silicon thin films by means of Berg-model handling the hydrogen incorporation as a reactive sputtering process involving ionization of molecular hydrogen followed by reactions between elemental target atoms to compound molecules. This approach is suitable for the interpretation of hydrogen incorporation into a-Si:H films based on the fact that the amount of incorporated hydrogen is proportional to the current. The imaginary and the real part of the dielectric function deduced from spectroscopic ellipsometry are investigated as a function of hydrogen flow. Using the results of spectroscopic ellipsometry and elastic recoil detection analysis presented earlier, as well as the equations of Berg model, the metal and compound sputtering rate and the sticking coefficient between silicon and hydrogen atoms are calculated. [N. Hegedüs, et al, *Interpretation of hydrogen incorporation into radio frequency sputtered amorphous silicon based on Berg modelling*, Vacuum, Volume 202, August 2022, 111164, https://doi.org/10.1016/j.vacuum.2022.111164 IF.: 4.11, Miklós Fried, Tivadar Lohner, Attila Németh, Péter Petrik, *In-situ measurement of changing complex dielectric function of ion implanted amorphous silicon during annealing by spectroscopic ellipsometry*, Invited lecture at ICSE-9, 9th International Conference on Spectroscopic Ellipsometry, 2022.05.22-26, Submitted to Thin Solid Films, 2022 August, TSF-D-22-00896]

WO_3-MoO_3 system

Reactive (Ar-O_2 plasma) magnetron sputtered WO_3-MoO_3 (nanometer scaled) mixed layers were investigated and mapped by Spectroscopic Ellipsometry (SE). The W- and Mo-targets were placed separately, and 30×30 cm glass substrates were slowly moved under the two (W and Mo) separated targets, see Fig. 5. We used different (oscillator- and Effective Medium Approximation, EMA-based) optical models to obtain the thickness and composition maps of the sample layer relatively quickly and in a cost-effective and contactless way. In addition, we used Rutherford Backscattering Spectrometry to check the SE results.

I. combinatorial deposition:

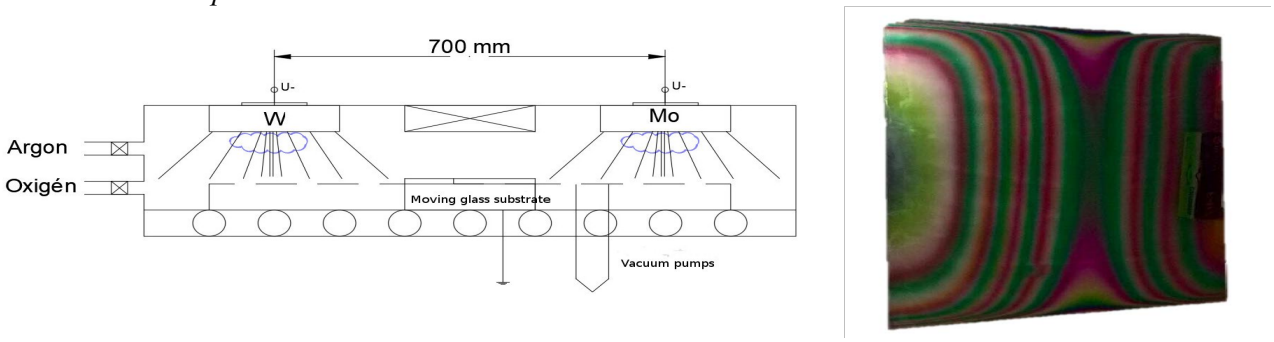

Fig. 5 *Schematic picture of the deposition arrangement and the photograph of 30x30cm substrate with composition-gradient layers. Newtonian rings show thickness gradient*

II. layer characterization

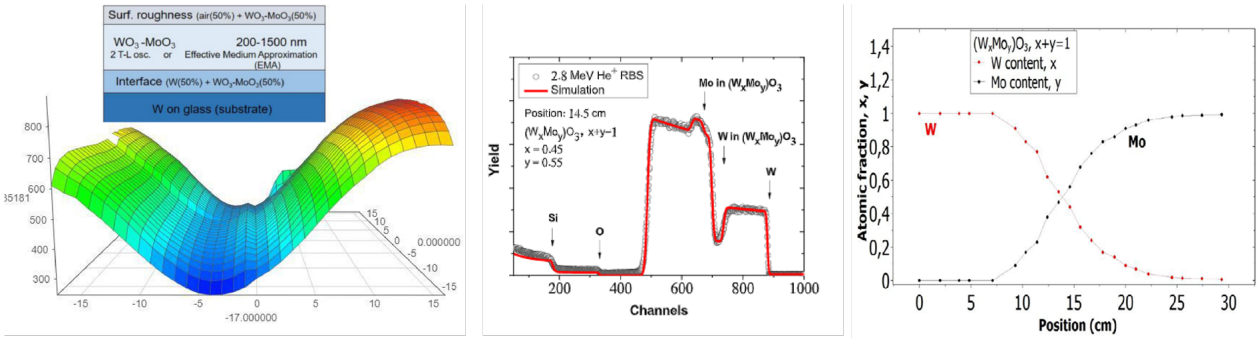

Fig. 6 *a., Ellipsometric thickness mapping of the combinatorial layer b., One Rutherford Backscattering Spectrometry example near the centre position. c., Composition-map along a line by Rutherford Backscattering Spectrometry*

Herein, we compare the "goodness" of different optical models depending upon the sample preparation conditions, for instance, the speed and cycle number of the substrate motion. Finally, we can choose between appropriate optical models (2-Tauc-Lorentz oscillator model vs. the Bruggeman Effective Medium Approximation, BEMA) depending on the process parameters. If one has more than one "molecular layer" in the "sublayers", BEMA can be used, see Fig. 7. If one has an atomic mixture, the multiple oscillator model is better (more precise) for this type of layer structure, see Fig. 8. [M. Fried, R. Bogar; D. Takacs; Z. Labadi; Z. E. Horvath; Z. Zolnai: *Investigation of Combinatorial WO_3-MoO_3 Mixed Layers by Spectroscopic Ellipsometry using Different Optical Models*, Nanomaterials 2022, 12(14), 2421; https://doi.org/10.3390/nano12142421] IF.: 5.719 (2021); Zoltán Lábadi, Dániel Takács, Peter Petrik, Miklós Fried, *Investigation of in- and out-diffusion of Li-ions in electrochromic tungsten-molybdenum oxide films by spectroscopic ellipsometry*, Poster lecture at ICSE-9, 9th International Conference on Spectroscopic Ellipsometry, 2022.05.22-26, Submitted to Thin Solid Films, 2022 August, TSF-D-22-00897

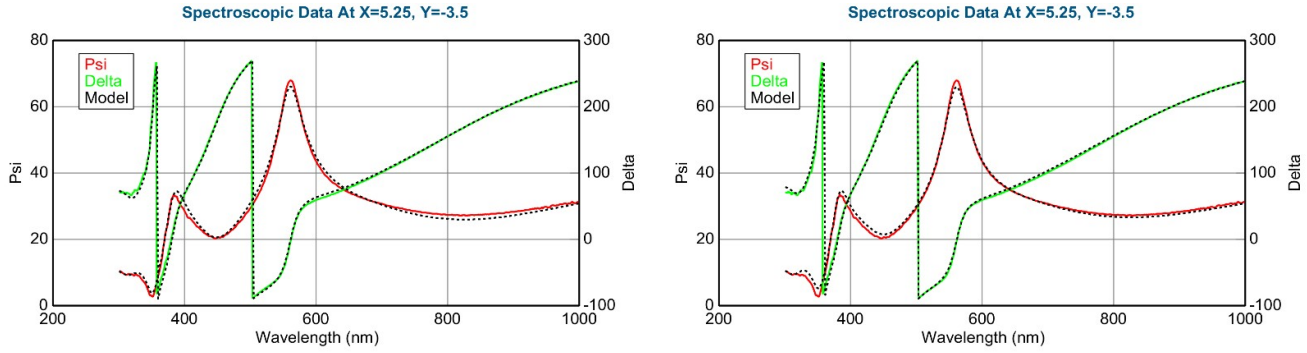

Figure 7 Measured and fitted spectra at one sample point: 2-Tauc-Lorentz (2-T-L) oscillator model. (a) Fit error (MSE) = 29.2, Thickness = 230.4 ± 0.8 nm, Amp1 = 58.0 ± 1.5, Amp2 = 11.4 ± 0.7, and Effective Medium Approximation model; (b) fit error (MSE) = 24.8, Thickness = 218.0 ± 0.1 nm, EMA% (Mat2) = 28.5 ± 1.3.

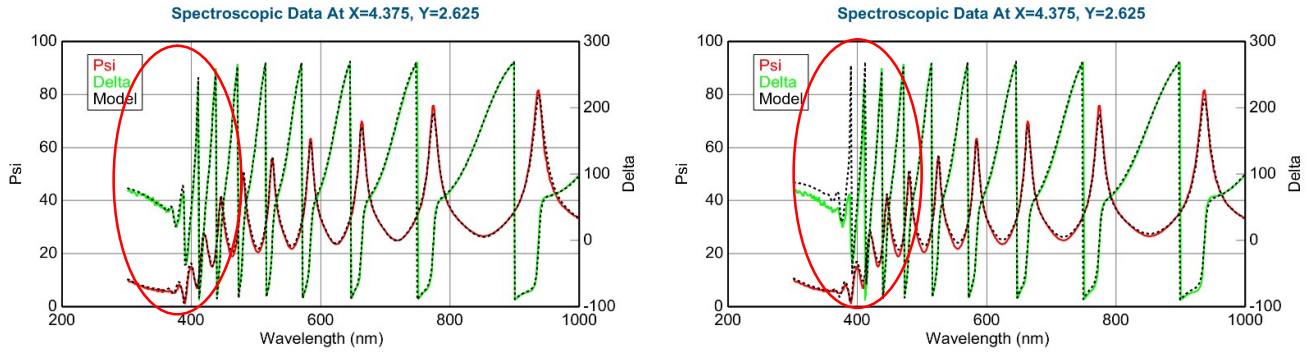

Figure 8 Measured and fitted spectra at one sample point: 2-Tauc-Lorentz (2-T-L) oscillator model. (a) Fit error (MSE) = 30.4, Thickness = 1159.6 ± 2.9 nm, Amp1 = 39.2 ± 1.1, Amp2 = 26.7 ± 0.4), and Effective Medium Approximation model; (b) fit error (MSE) = 40.1, Thickness = 1081.7 ± 2.8 nm, EMA% (Mat2) = 41.8 ± 0.8).

We have prepared two sets of (combinatorial) samples for VOC (Volatile Organic Compounds) sensing tests on heat-able sensor chips. Both contain 11 different pieces with different W/Mo ratio. See Fig. 9

Both sets are WoO_3/MoO_3 (lower) or WoO_{3-x}/MoO_{3-x} (upper) combinatorial sets, left hand side is W-rich, right one is Mo-rich. No. 6 (middle one) is expected to be 50-50% in both cases.

1., Upper row: suboxides (semi-transparent layers, No. 2 was broken during tweezer handling) see also Fig. 10 which shows the oxygen deficiency by EDS-SEM.

2. Bottom row: oxides (transparent layers)

The stoichiometric oxides were deposited at constant power mode, the suboxides at constant current mode.

Fig. 9 Photographs (from different view-angle) of WoO_3/MoO_3 (lower) or WoO_{3-x}/MoO_{3-x} (upper) combinatorial sets on heat-able sensor chips. Left hand side is W-rich, right one is Mo-rich. No. 6 (middle one) is expected to be 50-50% in both cases. The upper rows show suboxides (semi-transparent layers, No. 2 was broken during tweezer handling) The bottom rows show oxides (transparent layers)

Parallelly, control silicon samples were placed with the chips and spectroscopic ellipsometric measurements were applied to determine the actual thicknesses and composition. Fig. 11 shows the results of the control measurements. (Only the center part is shown where the composition is changing significantly. The precision of the results is less than 15 nm (thicknesses) and 5 % (composition) considering the changing values along one chip.

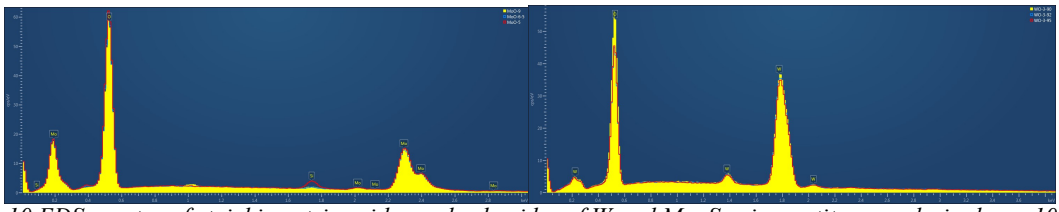

Fig. 10 EDS spectra of stoichiometric oxides and suboxides of W and Mo. Semi-quantitave analysis shows 10% oxygen vacancy

We performed a series of electrochromic measurements to optimize the Mo and W oxide composition for electrochromic behavior. The layers (prepared under the same conditions as on Fig. 5) on transparent conductive ITO layer-covered-glass were performed slow manner because of the virus pandemia.

The coloration efficiency (CE) of an electrochromic (EC) material is a critical factor for demonstrating its performance. The CE is defined as the change in optical density (ΔOD) per unit of the intercalated ionic charge (ΔQ) into an EC layer. CE and ΔOD can be obtained from the following equations:

$$\mathrm{CE} = \frac{\Delta \mathrm{OD}}{\Delta Q} \tag{1}$$

$$\Delta \mathrm{OD} = \log\left(\frac{T_b}{T_c}\right) \tag{2}$$

where T_b and T_c refer to the transmittances of the layer in its bleached and colored states, respectively.

We determined the layer thickness and composition values from SE measurements performed on the Si-probes which can be seen on Fig. 11 (center part of the upper-left side). The actual thickness and composition values are changing horizontally (Fig. 11, upper-right side). The CE parameters were determined from multiple measurements on multiple samples (Fig. 11 upper-left side) at many different wavelengths, using a Woollam M2000DI spectroscopic ellipsometer in direct transmission mode, registering the intensity values in-situ, real-time through an electrochemical cell. The CE values show clear optimum around 60 % (with 3 % uncertainty), see Fig. 11 central and lower pictures. The wavelength dependency was determined, too.

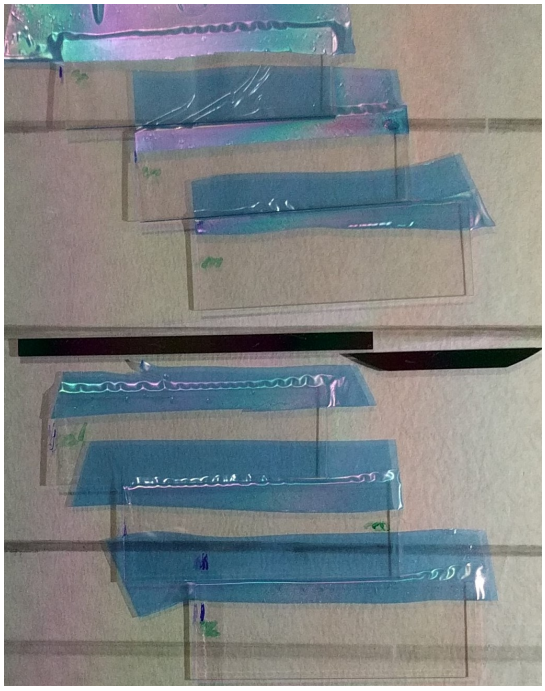

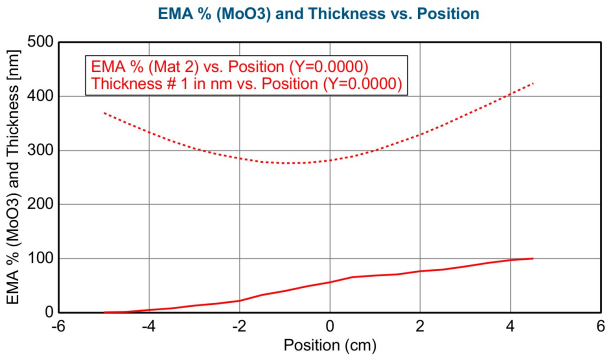

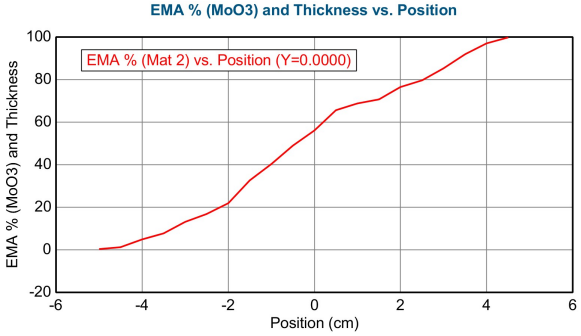

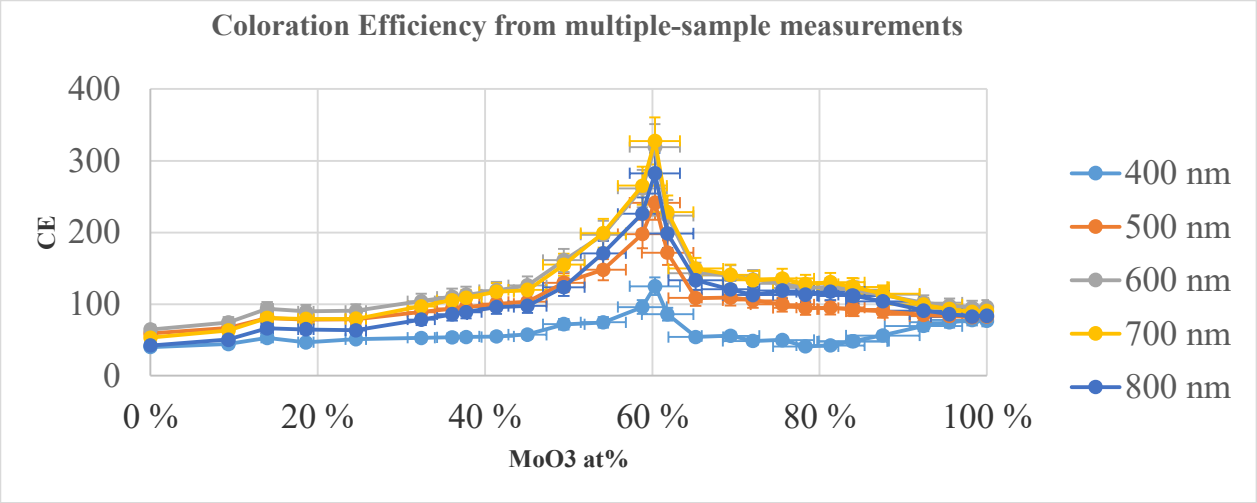

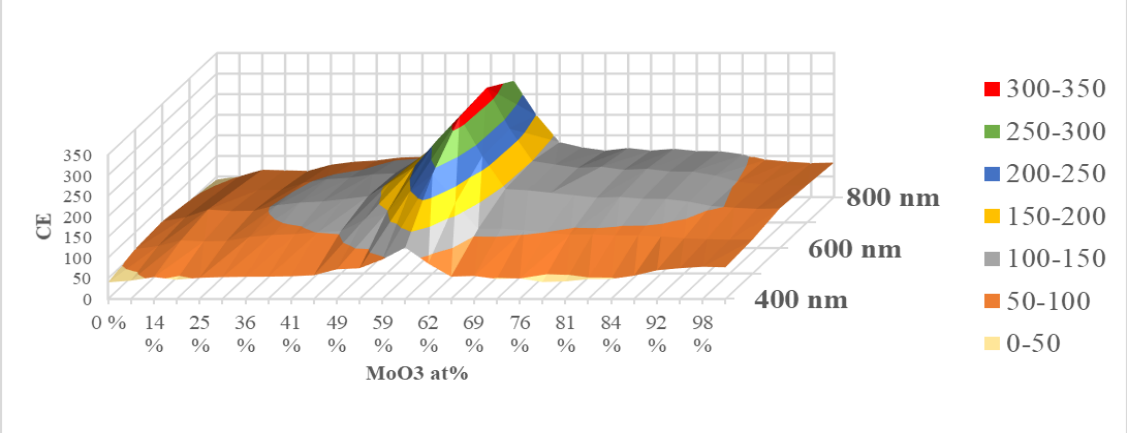

Fig. 11 Results of the control spectroscopic ellipsometric measurements (upper- right side) on the Si-probe (center part of upper-left photograph); CE parameters (central and lower picture) were determined from multiple measurements on multiple samples at many different wavelengths.

We finished the electrochromic measurements, we are writing the publication.

Ni-silicide phases in different compositions

Low-temperature solid-state reactions between Ni and Si were studied using in situ transmission electron microscopy (TEM). In the experiments thin amorphous silicon (a-Si) films were laid on Ni micro-grids and heated up to 973 K. In our approach the supporting Ni-grid serves as an unlimited source of nickel to successively form the whole range of Ni-silicide phases while diffusing into amorphous silicon. Unlike other thin film experiments where Ni and Si are layered on top of each other, our arrangement enables lateral diffusion of Ni along the Si layer and therefore enables the formation and study of successive Ni-Si phases side by side. That allowed us to observe in situ α-$NiSi_2$ as the first reaction product (see Fig. 12), in contrast to most studies that had reported either δ-Ni_2Si or θ-Ni_2Si as the first phase to form. α-$NiSi_2$ was continuously present at the reaction front propagating into the a-Si film. The phase sequence followed the increasing Ni concentration from a-Si towards the Ni-grid: α-$NiSi_2$, NiSi, Ni_3Si_2, δ-Ni_2Si, γ-$Ni_{31}Si_{12}$ and Ni_3Si. Almost all known Ni-silicide phases were found to form at relatively low temperatures except the θ-Ni_2Si, β-$NiSi_2$ and β3-Ni_3Si. The dominant phase was γ-$Ni_{31}Si_{12}$ which appeared in three structural modifications, differing in lattice periodicity along the c-axis. During our in situ heating experiments, in addition to the Ni-silicide layer formation a new phenomenon was observed, namely the appearance, growth and transformation of Ni-silicide whiskers (see Fig. 14) which was attributed to the accumulation of compressive stress in the thin layer. [E. Dodony, et al, *In situ TEM study of Ni-silicides formation up to 973K*, Journal of Alloys and Compounds Volume 918, 15 October 2022, 165466, https://doi.org/10.1016/j.jallcom.2022.165466 IF.: 6.371]

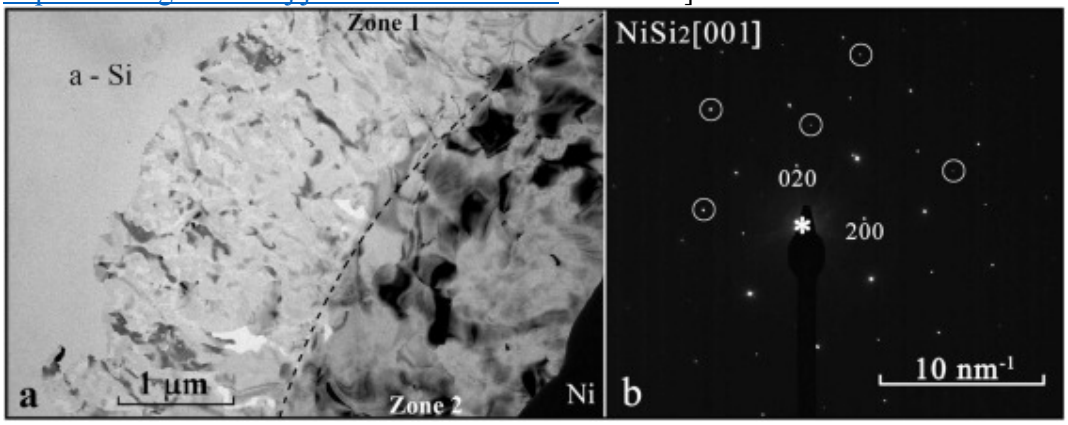

Fig. 12 (a) Bright field (BF) image of the reaction area showing a-Si, Zone 1, Zone 2 and Ni bar. The image was recorded at 873 K, 56 min after the beginning of solid-state reaction. (b) SAED pattern of a [001] oriented $NiSi_2$ grain imaged at Zone 1. The circled reflections come from other crystals nearby.

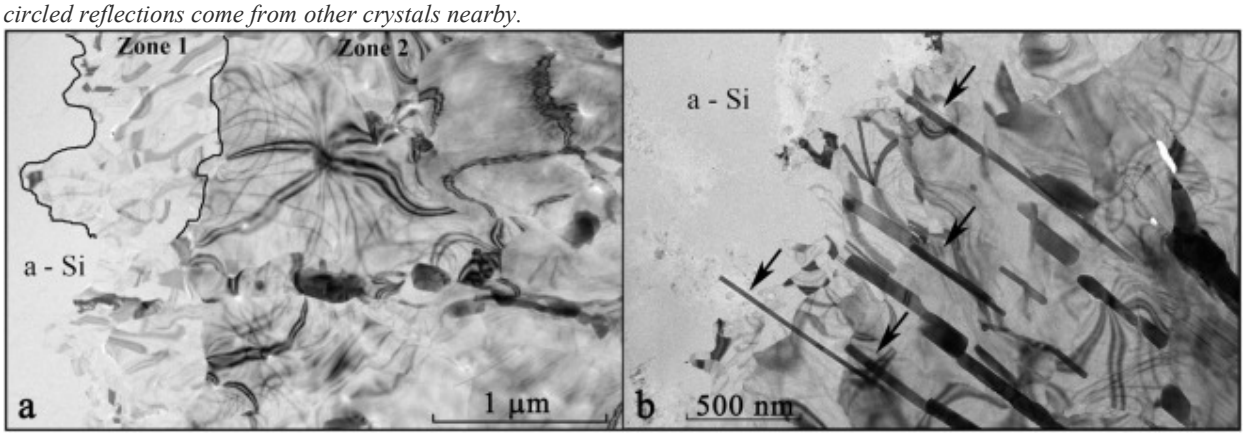

Fig. 13 (a) The borders between a-Si, reaction Zone 1 and reaction Zone 2, are marked with black lines on the bright field TEM image. (b) The bright field image of an area showing a bunch of parallel whiskers of various thickness (some of them are marked with arrows), protruding from the plane of the film at reaction Zone 2.

Y-Ti-O (perovskite) system

Materials with perovskite structure are receiving increasing attention in semiconductor research. They have a chemical formula ABX_3, where 'A' and 'B' are cations and X is an anion that bonds to both. A number of elements can be combined to form perovskite structure showing a wide variety of physical, optical, and electrical properties. From the large family of perovskites, we aimed to produce and characterize the Y-Ti-O system. Thin composition spread samples were deposited on carbon coated TEM grids by

reactive DC magnetron sputtering of yttrium and titanium in $3 * 10^{-3}\ mbar$ Ar gas with $1 * 10^{-4}\ mbar$ O_2 inlet. Using microcombinatory, we could produce and examine the oxides of the cations in the whole Y_xTi_{1-x} (x=0…1) concentration range in a single sample (Fig. 14).

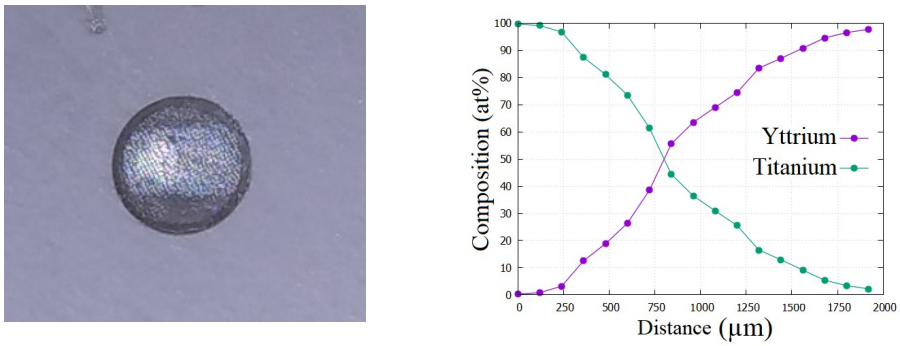

Figure 14 A combinatorial YTiO sample on a TEM grid and its EDS diagram representing concentration of the cations as a function of distance along the layer.

The microstructure as function of composition was determined by TEM and SAED: at high Y or Ti concentrations crystalline, while in between an amorphous structure was found (Fig. 15).

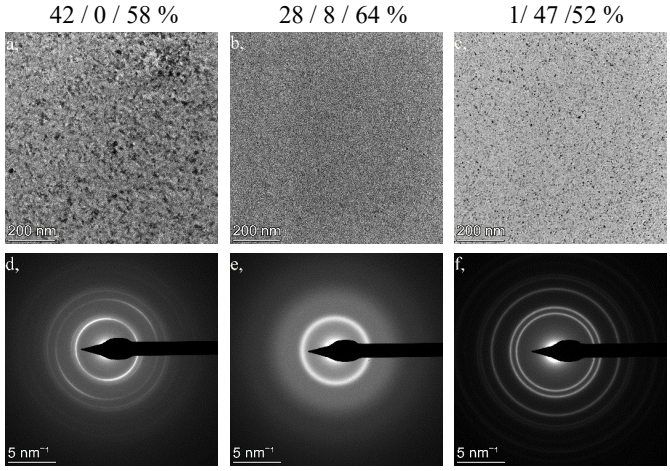

Figure 15 (a,b,c) BF TEM images of selected Y/Ti/O (at%) compositions (d,e,f) the corresponding SAED patterns. Sharp rings (d, f) show polycrystalline, while diffuse rings (e) represent amorphous structure.

Crystalline phases were determined by the evaluation of SAED measurements over the whole composition range with the help of the ProcessDiffraction software.

At the Ti surplus side of the sample, rocksalt-type cubic TiO structure was formed and the intensity of its characteristic peaks decreases with the increase of Y concentration. Between Y/Ti/O 14/28/58 and 28/8/64 at% compositions only diffuse peaks are present, characteristic for amorphous structure. With a further increase of the Y content, at 33/5/62 at% composition, the peaks of the Y_2O_3 crystalline phase appears. At even higher Y concentration (33/5/62) additional small peaks appear representing a Mn_2O_3 bixbyite-type cubic structure of Y_2O_3. [D. Olasz, et al, *Microstructure of composition spread YTiO thin films*, In: Fried, M. (ed.) Symposium on Materials Science, Mátraháza, Magyarország : Óbudai Egyetem (2022) pp. 29-30.]

We started the perovskite investigations with this combinatorial YTiO system. We performed a continuous annealing (2 C/min between Rt-600 C) and in-situ, real-time SE measurement along the central line of the sample at atmospheric ambient. Data analysis is ongoing and publication of the results is planned.

After performing the in-situ SE measurement series, we measured the position-dependent composition along the central line of the sample, determining the end-state. (See Fig. 16)

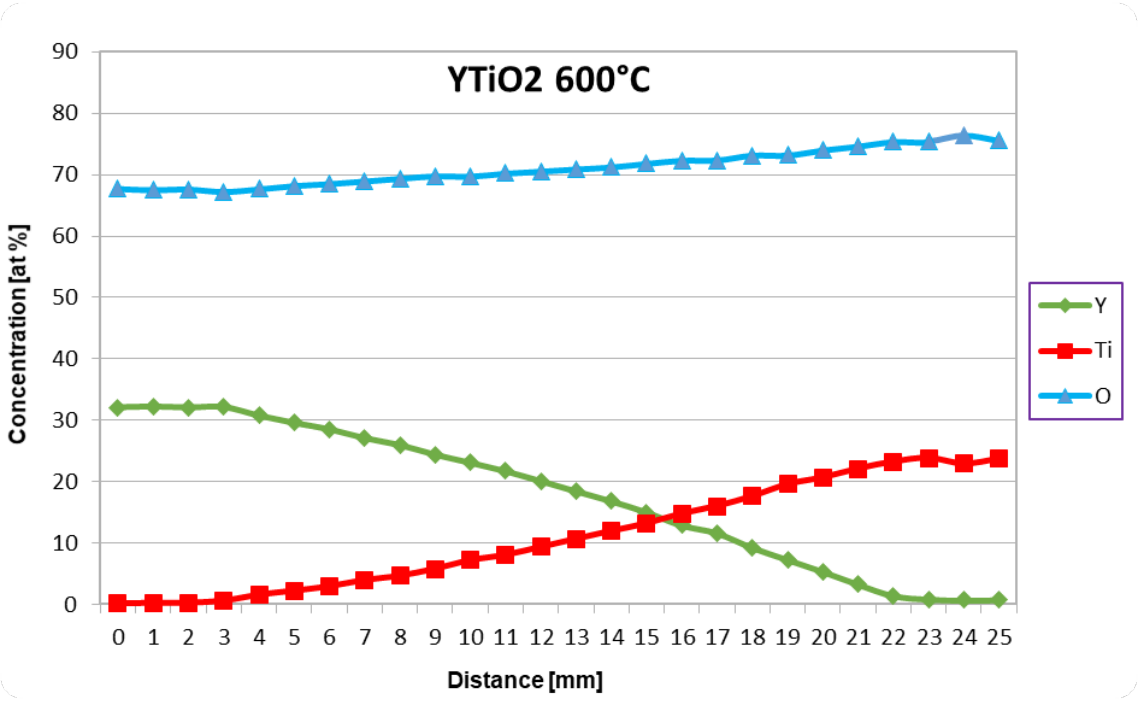

Fig. 16 EDS measurement in the electron microscope showing the position-dependent composition

We can see a continuous change in the composition between 3 and 23 mm position. We can see a continuous oxygen contain-change from the Y-side to the Ti-side which is understandable considering the stoichiometric Y_2O_3 (1Me, 1.5 oxygen) and stoichiometric TiO_2 (1Me, 2 oxygen) compositions.

The in-situ SE mapping series (full time: 5.5 h, 120 line scans between -12 mm - 12 mm with 1 mm steps, 2x3 s/point, 2880 points from RT to 600 C) resulted a series of the line scans at different (quasi-static) temperatures. (Temperature-change during one line scan is less than 5 C.)

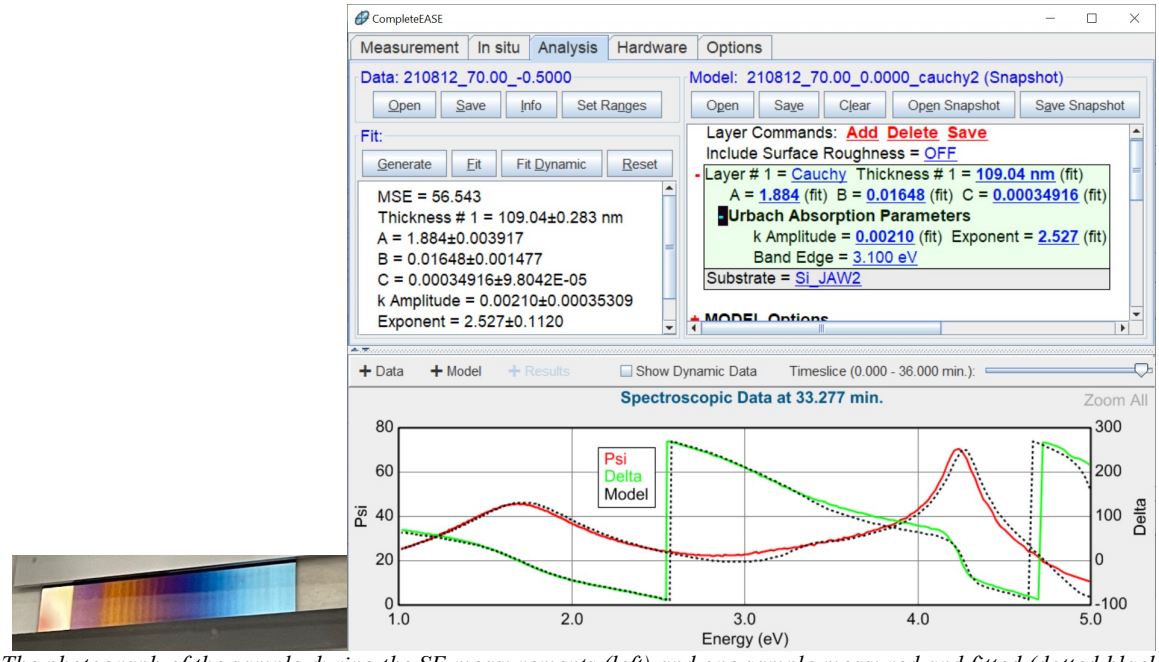

Fig. 17 The photograph of the sample during the SE measurements (left) and one sample measured and fitted (dotted black line) spectrum-pair plus the optical model.

As a first evaluation (first overseeing of the temperatures and compositions where phase change can be seen) we used a simple, one-layer, Cauchy-dispersion optical model (Fig. 17). The optical model is good enough only for the layers where the phase change has happened.

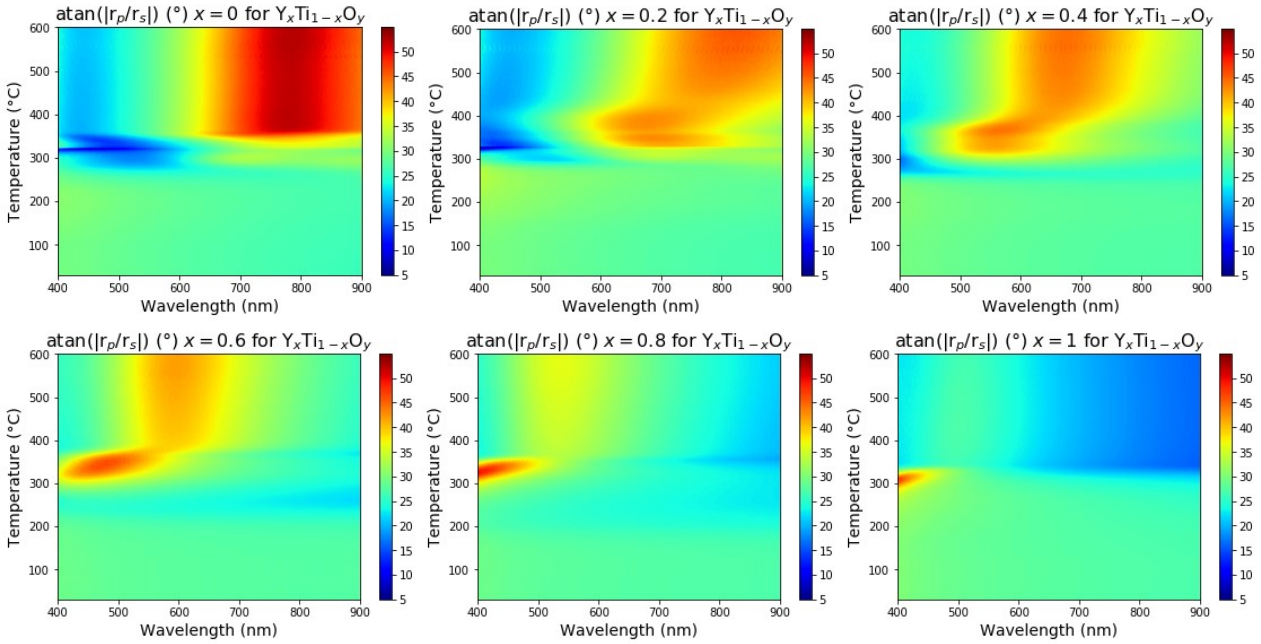

Fig. 18 Full spectral maps (spectral response at each temperatures) at different compositions. x=0, 0.2, 0.4, 0.6, 0.8, 1 for $Y_xTi_{1-x}O_y$

On the Fig. 18, one can see spectral maps at different points (different compositions) of the sample. This spectral responses show a complex response of the sample, showing the change in the complex refractive index and the thickness together. It is very obvious, where (which composition and which temperature) is the phase change. (Still working on the evaluation.)

Mapping and imaging of thin films on large surfaces

Thin films covering large surfaces are used in a very wide range of applications from displays through corrosion resistance, decoration, water proofing, smart windows, adhesion performance to solar panels, and many more, for instance to map combinatorial samples. Scaling up existing thin-film measurement techniques requires a high speed and the redesign of the configurations. We published a review article to give an overview of recent and past activities in the area, as well as an outlook of future opportunities. Only two methods have been identified that are capable of mapping or imaging meter-sized areas. One of them moves an ellipsometry head over the surface utilizing point-by-point mapping. Divergent light source macro-imaging SE is, however, capable of increasing the speed of large-area measurement by at least an order of magnitude utilizing imaging, measuring multiple points over the surface simultaneously by SE, and maintaining the capabilities of complex modeling and nanometer-scale sensitivity [Petrik, Peter and Fried, Miklos, *Mapping and imaging of thin films on large surfaces*, PHYSICA STATUS SOLIDI A-APPLICATIONS AND MATERIALS SCIENCE, Volume 219, Issue13, Article Number 2100800, Published: JUL 2022, https://doi.org/10.1002/pssa.202100800 IF.: 2.170 (2021) Document Type: Review; Berhane Nugusse, György Juhász, Csaba Major, Péter Petrik, Sándor Kálvin, Zoltán György Horváth, Miklós Fried, *Non-destructive optical mapping tool from cheap parts*, Poster lecture at ICSE-9, 9th International Conference on Spectroscopic Ellipsometry, 2022.05.22-26, Submitted to Thin Solid Films, 2022 August, TSF-D-22-00891]

Al/Ag and Mn/Ag systems

The demand for further improvement in the field of label-free biosensing is one of the most crucial topics of life science nowadays. For this purpose, numerous optical methods and combined techniques have been developed and new sensing structures have also been introduced in the last couple of years.

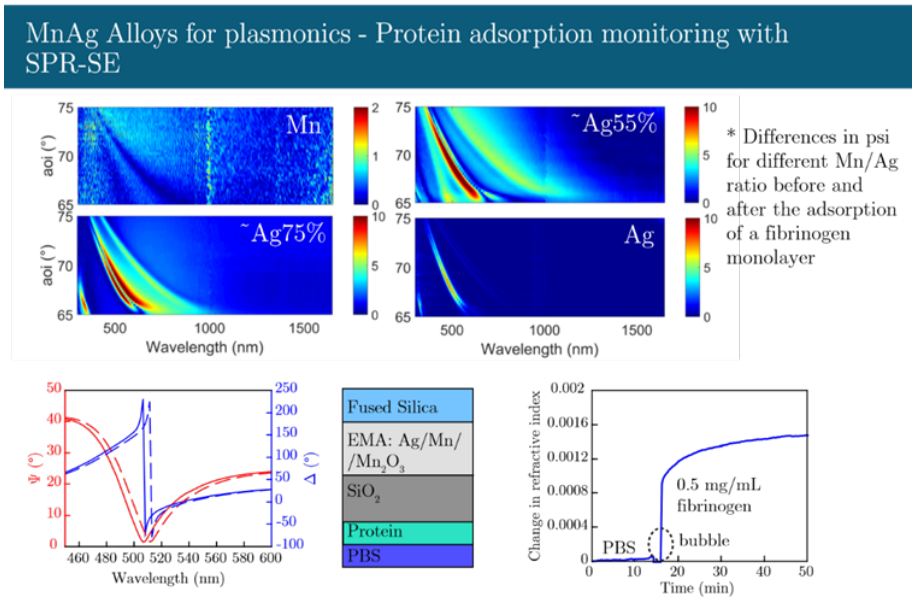

Fig. 19 *Differences in psi for different Mn/Ag ratio before and after the absorption of a fibrinogen monolayer*

We tried to use silver and silver based alloy layers instead of plasmonic gold, since silver has more favorable properties regarding to biosensing purposes. (See Fig. 19 and B. Kalas, et al, „*Combinatorial Biosensing by Total Internal Reflection Spectroscopic Ellipsometry*", 42nd International Semiconductor Conference CAS 2019 Sinaia, Romania, 9 - 11 October 2019, oral presentation) We studied a novel layer system consisting of an alloy layer of silver and aluminium or manganese and also a SiO_2 or Si_3N_4 waveguide layer on top of it. The alloy layer was realized with the micro-combinatorial sputtering technique (see Fig. 20 left a) that makes possible that all the possible composition values of the two materials (from 100% silver to 100% manganese or aluminium, with linear change along the sample) are presented only on one sample. Subsequently the biosensing properties of this layer was demonstrated by a combined SPR-SE measurement of a protein adsorption process. The sensitivity of the method is in the 10^{-5} - 10^{-6} range (RI).

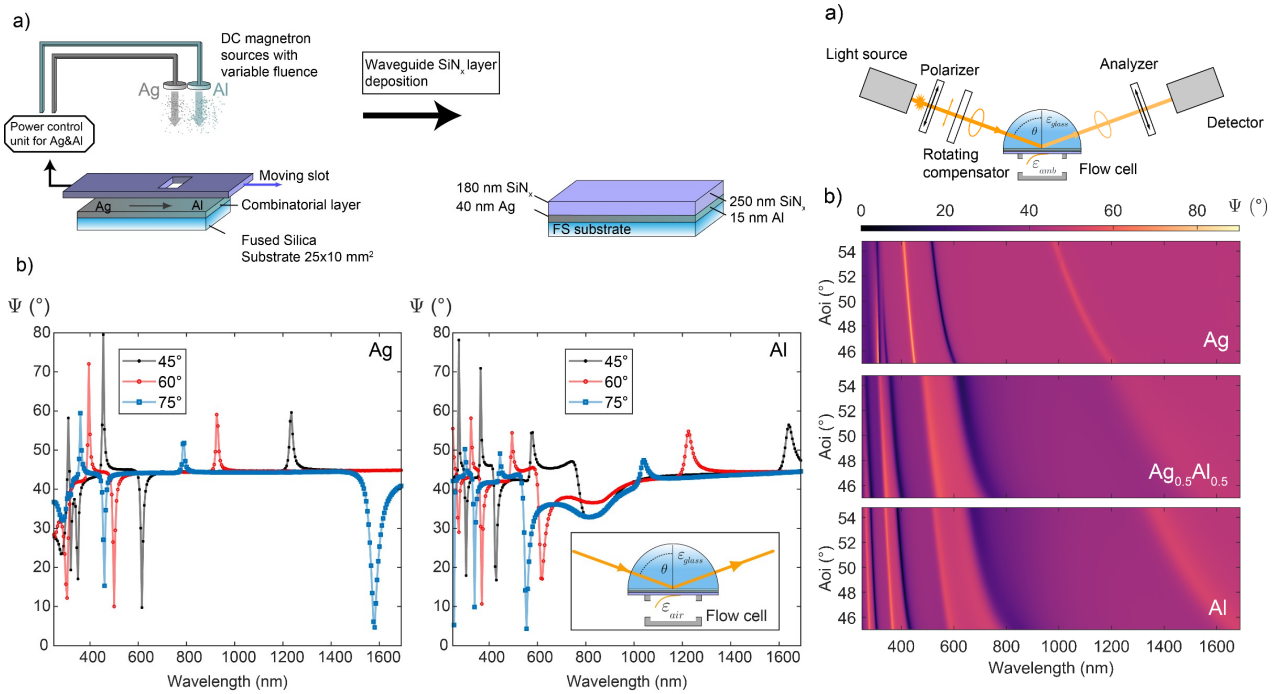

Fig. 20 Compositional grading of plasmonic ultrathin combinatorial Ag_xAl_{1-x} layer combined with waveguide layer can provide multiple spectral positions of the resonance in a wide wavelength range from the UV to NIR by using phase-sensitive Kretschmann-Raether ellipsometry. Left a) shows the preparation method b) shows example spectra at different angle-of-incidences with tunable resonance peaks. Right a) shows the measuring configuration b) shows the resonance peak position at different compositions.

Plasmonic $Mn/Ag/SiO_2$ and $AgAl/Si_3N_4$ sensor layer structures were deposited (and investigated) on fused silica glass slide by dual DC magnetron sputtering, see Fig. 19 and 20 left a). The composition of the layers were

laterally graded in which x linearly changes from x = 0 to x = 1 over a distance of 20 mm. The SiO_2 and Si_3N_4 layers serve both as a resonator and a protective layer providing homogeneous chemical properties on top of the inhomogeneous AgAl layer. The structures were illuminated through a hemi-cylinder for variable-angle measurements in the Kretschmann-Raether (KR) configuration using a focused spot that enabled the change of x by moving it along the gradient of the composition, see Fig. 20 right a). Optical properties of layers in the whole composition range were obtained. The positions of resonant peaks were shifted by changing the angle and the lateral position of the spot in a flow-cell configuration. Based on the capabilities of ellipsometry limit of detection in refractive index unit values of $\approx 4 - 8 \times 10^{-6}$ can be achieved in the resonant positions utilizing both p- and s-polarizations in the case of $AgAl/Si_3N_4$ sensor layer. Due to the flexible tunability of the resonant wavelengths by moving a focused spot, the above sensitivity is available in-situ, over the spectral range of 265-1504 nm, in the UV-VIS-NIR wavelength ranges.

Our multi-spot, multi-angle tool with the compositionally graded surface realizes a ”scanning resonant wavelength” capability, in which the spectral position of the highest sensitivity can be adjusted during the in-situ measurement, see Fig. 20 b). [B. Kalas, et al, "*Development of advanced sensing materials and interface structures for in-situ bioellipsometry*", Proc. SPIE 11972, Label-free Biomedical Imaging and Sensing (LBIS) 2022, 119720G (2 March 2022); https://doi.org/10.1117/12.2609882 IF.: 0.38 (2021); B. Kalas, et al, *Surface-enhanced Kretschmann-Raether ellipsometry based on plasmonic, Bragg and waveguide structures*, In: Fried, M. (ed.) Symposium on Materials Science, Mátraháza, Magyarország : Óbudai Egyetem (2022) pp. 12-14.; B. Kalas, et al, *Scanning-resonance optical sensing based on a laterally graded plasmonic layer – optical properties of Ag_xAl_{1-x} in the range of x = 0 to 1*, B. Kalas, G. Safran , M. Serenyi , M. Fried, P. Petrik, *Scanning-resonance optical sensing based on a laterally graded plasmonic layer – optical properties of Ag_xAl_{1-x} in the range of x = 0 to 1*, Applied Surface Science, Volume 606, 30 December 2022, 154770 http://dx.doi.org/10.2139/ssrn.4107340]

Amorphous oxynitride systems

We further optimized the RF sputtering system using a smart gas dosage for the sputter deposition to use them for combinatorial material synthesis. (See Fig. 21 and G. Sáfrán, et al; „*Smart gas dosage by a peristaltic pump for reactive RF sputtering of composition spread combinatorial hafnium-oxy-nitride layers*”; Vacuum 182 (2020) 109675) We prepared composition spread metal oxy-nitride combinatorial layers by reactive radiofrequency sputtering for a highly efficient characterization of their optical properties in a wide range of O/N ratios. Affinity of metals requires oxygen proportion, in the Ar-O-N plasma, be set orders of magnitude lower compared to nitrogen. The required low partial pressure range of oxygen was covered by a new concept self-regulating gas inlet assembly based on a peristaltic pump delivering gas from a finite volume vial. Accordingly, oxygen partial pressure was gradually decreasing from 8×10^{-5} mbar towards base pressure of the chamber.

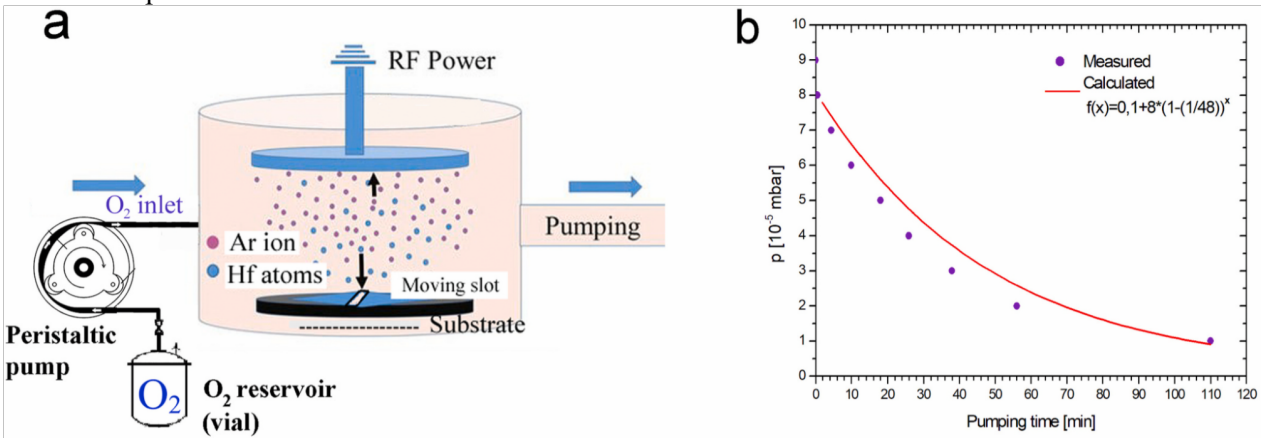

Fig. 21 (a) Setup of the self-regulating gas inlet system that consists of a vial connected to a peristaltic pump. (b) Variation of oxygen partial pressure vs. time in the sputtering chamber achieved by the self-regulating gas inlet. The peristaltic pump was operated at a constant rate of 1 sccm emptying the 48 cm^3 vial of 1 bar initial pressure. Full circles: measured pressure decay. Solid line: calculated pressure decay according to equation

This assembly effected a continuous oxygen depletion and a transition of the deposited film from oxide to nitride. The suitability of our combinatorial method was proved by both energy dispersive spectrometry mapping and Spectroscopic Ellipsometry (SE) of the correlated refractive indices along a composition-spread HfON sample. These results open up new opportunities for efficient, combinatorial characterization

of the composition dependent properties of RF sputter deposited Me-oxy-nitride layers based on various metals.

Next, in a single technological process, an amorphous silicon oxynitride layer was grown, which includes the entire transition from oxide to nitride. The variation of the optical properties and the thickness of the layer was characterized by Spectroscopic Ellipsometry (SE) measurements, while the elemental composition was investigated by Energy Dispersive Spectroscopy (EDS). It was revealed that the refractive index of the layer is tunable in the 1.48 – 1.89 range by varying the oxygen partial pressure in the chamber. From the data of the composition of the layer, the typical physical parameters of the process were determined by applying the Berg model valid for reactive sputtering. In the modelling, a new approach was introduced, where the metallic Si target sputtered with a uniform nitrogen and variable oxygen gas flow was considered as an oxygen gas-sputtered SiN target. The layer growth method used in the present work and the revealed correlations between sputtering parameters, layer composition and refractive index, enable both to achieve the desired optical properties of silicon oxynitride layers (see Fig. 22) and to produce thin films with gradient refractive index for technology applications. [N. Hegedüs, et al, *Investigation of the RF sputtering process and the properties of deposited silicon oxynitride layers under varying reactive gas conditions*, Materials 2022, 15, x. https://doi.org/10.3390/xxxxx IF.: 3.748 (2021)]

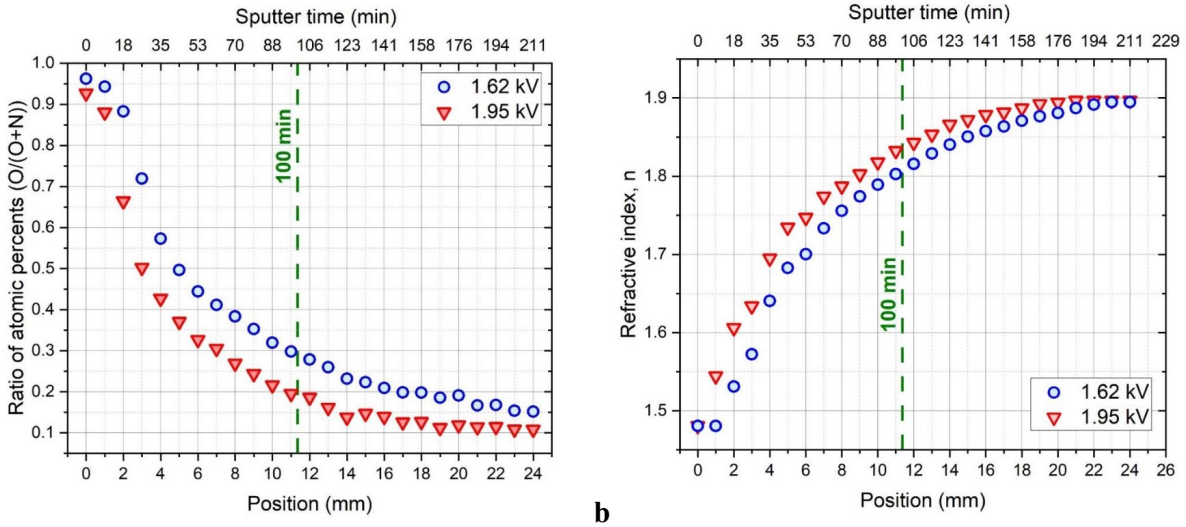

Figure 22 a) Ratio of atomic concentrations (O/O+N) determined by EDS measurements along the composition spread samples deposited at 1.62 and 1.95 kV wall potential b) Refractive index (n) of the composition spread samples measured along the substrate by spectroscopic ellipsometry

a-SiNx:H system

Amorphous hydrogenated silicon nitride thin films (a-SiNx:H) have widespread applications from device passivation to light emitting diodes and antireflective coatings for solar cells. Chemical vapor deposition (CVD) and physical vapor deposition (PVD) are the most common techniques for silicon nitride film deposition with or without hydrogen addition. CVD-deposited film always contains hydrogen and its amount cannot be controlled directly during the preparation process. Due to this fact, the alternative fabrication method for controlled hydrogen concentration in a direct way from zero hydrogen content by adjusting the applied hydrogen gas flow to the chamber could be PVD (e.g., RF sputtering).

We sputtered a-SiNx:H films at various H2 flows with average thickness of 150 nm, and the effect of hydrogen incorporation on structural and optical properties was studied, see Fig. 22. The detailed structural characterization confirmed the formation of a dense thin film at hydrogen-free sputtering and a porous structure with homogenously distributed nanometer-scale porosities caused by hydrogen addition. The refractive index of 1.96 was characteristic for hydrogen-free SiNx thin films. Hydrogen flows up to 3 sccm were found to have no or minimal effect on the refractive index; for flows from 6 to 12 sccm, the refractive index decreased from 1.96 to 1.89, which can be explained by the hydrogen and nitrogen incorporation into the thin films. The calculations from FTIR spectra showed that a-SiNx:H sputtered at 6 sccm H2 flow presented a concentration of bounded hydrogen of ~4 at.%. The ERDA measurements confirmed a total hydrogen content of 10 at.%. This means that 6 at.% hydrogen was incorporated in a molecular form during the layer growth, which explained the lower density of the thin films. The out-diffusion of hydrogen due to annealing plays a prominent role in the densification of thin films. The molecular form of hydrogen is

released at a temperature of ~65 °C from the film. Blisters with 100 nm diameter are created on the surface of the thin films. The low activation energy calculated by the Arrhenius method refers to significant diffusion of hydrogen molecules. [N. Hegedüs, et al, *Examination of the Hydrogen Incorporation into Radio Frequency-Sputtered Hydrogenated SiN_x Thin Films* COATINGS 11 : 1 Paper: 54 , 13 p. (2021)]

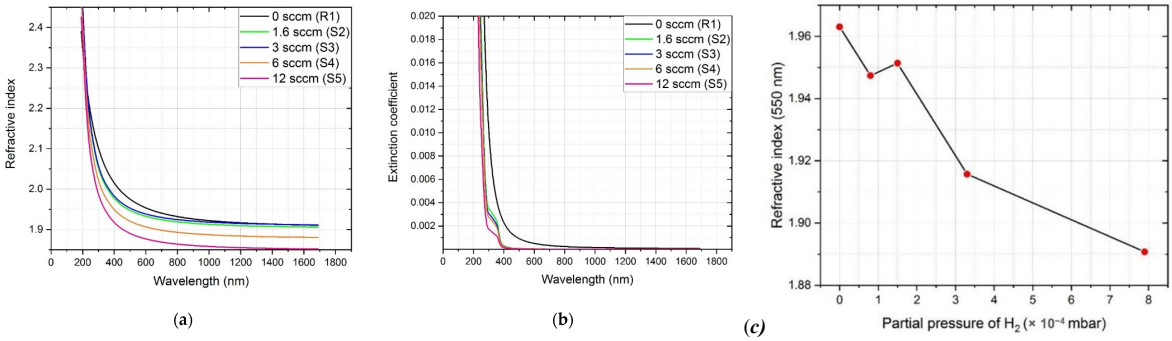

*Fig. 22 Effect of hydrogen flow on the optical properties of SiN_x:H thin films: (**a**) refractive index, (**b**) extinction coefficient. (**c**) Refractive index of hydrogenated silicon nitride (SiN_x:H) thin films at a wavelength of 550 nm as a function of H_2 partial pressure.*

$Cr_xAl_{1-x}N$ system

CrAlN alloys can play an important role in the improvement of next generation piezoelectric MEMS devices. However, enhanced piezoelectric constants require high degree of uniaxial orientation in the polycrystalline thin film. In this work, $Cr_xAl_{1-x}N$ thin films with varying compositions were deposited at different substrate temperatures by reactive DC co-sputtering technique and compared with respect to their microstructure and optical properties. The relationship between the atomic composition of the layers and the plasma powers over the Al and Cr targets during co-sputtering was revealed accurately by Rutherford backscattering spectrometry. As it was found by X-ray and selective area electron diffraction methods, thin films in the range of $x = 0–0.23$ show hexagonal wurtzite-type phase, which changes to cubic rock-salt-type structure between $0.23 < x < 0.31$. At lower Cr cation concentration, like $x = 0.12$ the wurtzite-type polycrystalline film indicates uniaxial texture, whereas it is almost randomly oriented at $x = 0.23$. (See Fig. 23 a) Among the compared compositions, $Cr_{0.12}Al_{0.88}N$ showed the strongest c-axis orientation, whereas the optimal substrate temperature was found to be $T = 350$ °C. While the refractive index measured by ellipsometry increases monotonously from 2.07 to 2.64 with increasing Cr cation concentration in the range of $x = 0–0.31$, the optical bandgap shrinks from 2.65 to 2.23 eV, see Fig. 23 b. These optical data can provide references for future contactless wafer-scale optical monitoring process. (Soleimani, S., et al, J. *Optimization of co-sputtered $Cr_xAl_{1-x}N$ thin films for piezoelectric MEMS devices*. J Mater Sci: Mater Electron 31, 8136–8143 (2020))

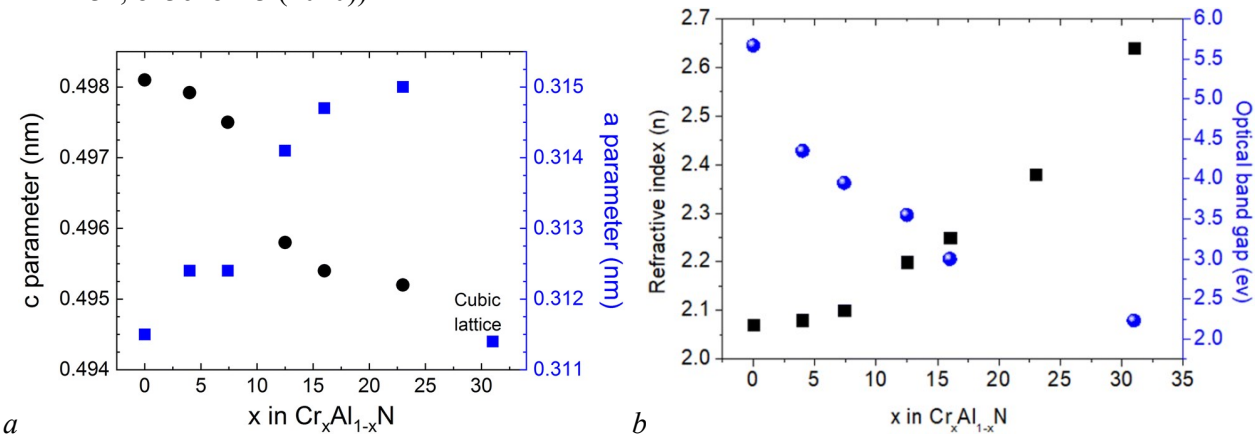

Fig. 23 Lattice parameter values of c and a (a) Refractive index (n) and optical bandgap measured by ellipsometry at the wavelength of 633 nm as a function of the Cr concentration in $Cr_xAl_{1-x}N$ thin films (b)

Al–Mg films

We prepared ultrafine-grained Al–Mg films and investigated them by Transmission Electron Microscopy (TEM), Atomic Force Microscopy (AFM), and nanoindentation. It was revealed that these films have extremely high strength, enabling their potential application as protecting layers. Besides the possible practical applications, the results of the present work also confirm the validity of the modified Hall–Petch

relationship for the uniform description of the strength of face-centered cubic metals and solid solution having ultrafine-grain size. Nguyen Q. Chinh, György Sáfrán: High strength of ultrafine-grained Al–Mg films and the relevance of the modified Hall–Petch-type relationship, MRS Communications 9, 1111–1114 (2019). https://doi.org/10.1557/mrc.2019.108

Publications:

G. Sáfrán, T. Lohner, M. Serényi, P. Petrik, B. Kalas, Z. Zolnai, M. Fried, J. Gubicza, N.Q. Chinh: A micro-combinatorial approach for a reveal of composition dependent properties of binary films by TEM and further analytical techniques, Oral presentation (invited), 6th_International Congress on Microscopy and Spectroscopy Oludeniz, Turkey, May 12-18, 2019 Conference proceedings

G. Sáfrán, T. Lohner, M. Serényi, P. Petrik, B. Kalas, Zs. Zolnai, M. Németh, J. Gubicza , N.Q. Chinh , M. Fried, G. Dobrik. I. Cora, Zs. Fogarassy, L.J. Lábár, N. Szász: One-sample concept" micro-combinatory; a new approach for high throughput characterization of binary films, Oral presentation (invited), International Conference on Material Science and Nanotechnology(ICMSN 2019) , Paris, France, September 17-18, 2019, Conference proceedings

G. Sáfrán, T. Lohner, M. Serényi, P. Petrik, B. Kalas, Zs. Zolnai, M. Németh, J. Gubicza, N. Chinh: Single-sample combinatory for high throughput TEM, RBS, XRD, nanoindentation and ellipsometry studies of binary films, Oral presentation (invited), 26th Assembly of Advanced Materials Congress (AMC), Stockholm Sweden, 10-13 June 2019, Conference proceedings

György Sáfrán, Benjámin Kalas and Miklós Serényi: Determination of the optical properties of a-SixGe1-x facilitated by micro-combinatory, Poster and Proceedings, 15TH INTERNATIONAL CONFERENCE OF COMPUTATIONAL METHODS IN SCIENCES AND ENGINEERING, Rhodes, Greece May 1-5 2019, Conference proceedings

M. Fried: Expanded Beam Spectro-Ellipsometry for Big Area On-line Monitoring, nvited lecture, International Congress on Advanced Materials Sciences and Engineering (AMSE-2019), Osaka, Japán, 2019.07.22-2019.07.24, 2019 Conference article

Nguyen Q. Chinh, György Sáfrán: High strength of ultrafine-grained Al–Mg films and the relevance of the modified Hall–Petch-type relationship, MRS Communications MRSCOM-2019-0084.R1 Research Letter, 27 August 2019, pp. 1-4, IF.: 1.935

T. Lohner, E. Szilágyi, Z. Zolnai, A. Németh, P. Petrik, Z. Fogarassy, L. Illés, E. Kótai, M. Fried: Determination of complex dielectric function of ion-implanted amorphous germanium by spectroscopic ellipsometry, ICSE-8, 8. Int. Conf. on Spectroscopic Ellipsometry, 2019.05.26-31 Barcelona, poster presentation; article submitted to Journal of Vacuum Science & Technology, 2019 Conference article

Benjamin Kalas, Zsolt Zolnai, György Sáfrán, Miklós Serényi, Emil Agocs, Tivadar Lohner, Attila Nemeth, Nguyen Quoc Khanh, Miklós Fried, and Peter Petrik: Micro-combinatorial sampling of the optical properties of hydrogenated amorphous Si1−xGex for the entire range of compositions towards a database for optoelectronics, SCIENTIFIC REPORTS 10 : 1 Paper: 19266 , 19 p. (2020), Article in periodical IF.: 4.130

György Sáfrán, Noémi Szász, Gergely Dobrik, Benjámin Kalas, Miklós Serényi: Smart gas dosage by a peristaltic pump for reactive RF sputtering of composition spread combinatorial hafnium-oxy-nitride layers, Vacuum 182 (2020) 109675, DOI: 10.1016/j.vacuum.2020.109675, 2020 Article in periodical IF.: 2.670

György Sáfrán, Noémi Szász, Gergely Dobrik, Benjámin Kalas, Miklós Serényi: Self-regulating gas dosage for reactive RF sputtering of composition spread Hf oxy-nitride combinatorial layers, In: Miklós Fried (szerk.) Proceedings of Anyagtudományi Szimpózium, Budapest, Magyarország: Óbudai Egyetem (2020) 44 p. pp. 41-44., 2020 Conference proceedings

Ildikó Cora, János L. Lábár, György Sáfrán: Concentration dependent pair-correlation in amorphous Si1−xGex layers revealed by micro-combinatorial TEM, In: Miklós Fried (szerk.) Proceedings of Anyagtudományi Szimpózium, Budapest, Magyarország, Óbudai Egyetem (2020) 44 p. pp. 26-30., 2020 Conference proceedings

Lohner, T; Szilágyi, E; Zolnai, Zs; Németh, A; Fogarassy, Zs; Illés, L; Kótai, E; Petrik, P; Fried, M: Determination of the Complex Dielectric Function of Ion-Implanted Amorphous Germanium by Spectroscopic Ellipsometry, COATINGS 10 : 5 Paper: 480 , 10 p. (2020) https://doi.org/10.3390/coatings10050480, Article in periodical IF.: 2.436

M. Fried, R., Bogar, Z. Lábadi, Z. E. Horvath, Z. Zolnai: Combinatorial Investigation of WO3-MoO3 Mixed Layers by Spectroscopic Ellipsometry to assess Effective Medium Approximation, In: Miklós Fried

(szerk.) Proceedings of Anyagtudományi Szimpózium, Budapest, Magyarország : Óbudai Egyetem (2020) 44 p. pp. 3-10., 2020 Conference proceedings

Soleimani, S., Kalas, B., Horváth, Z., Zolnai, Z., Czigány, Z., Németh, A., Petrik, P., Volk, J.: Optimization of co-sputtered CrxAl1−xN thin films for piezoelectric MEMS devices, Journal of Materials Science: Materials in Electronics 31, 8136–8143 (2020), Article in periodical IF.: 2.376

Z. Labadi, P. Petrik M. George, C. Moldovan, M. Fried: Preparation and Characterization of Mixed Metal Oxide Layers using Reactive Combinatorial Sputtering, In: Miklós Fried (szerk.) Proceedings of Anyagtudományi Szimpózium, Budapest, Magyarország : Óbudai Egyetem (2020) 44 p. pp. 31-33., Conference proceedings

Kalas B, Ferencz K, Saftics A, Czigany Z, Fried M, Petrik P: Bloch surface waves biosensing in the ultraviolet wavelength range - Bragg structure design for investigating protein adsorption by in situ Kretschmann-Raether ellipsometry, APPLIED SURFACE SCIENCE 536: 147869, 2021 Article in periodical IF.: 4.130

Nikolett, Hegedűs ; Riku, Lovics ; Miklós, Serényi ; Zsolt, Zolnai ; Péter, Petrik ; Judit, Mihály ; Zsolt, Fogarassy ; Csaba, Balázsi ; Katalin, Balázsi: Examination of the Hydrogen Incorporation into Radio Frequency-Sputtered Hydrogenated SiNx Thin Films, COATINGS 11 : 1 Paper: 54 , 13 p. (2021), Article in periodical IF.: 2.864

Benjamin Kalas, Gyorgy Safran , Miklos Serenyi , Miklos Fried, Peter Petrik: Scanning-resonance optical sensing based on a laterally graded plasmonic layer – optical properties of AgxAl1−x in the range of x = 0 to 1, Applied Surface Science, Volume 606, 30 December 2022, 154770, Article in periodical IF.: 7.392

Benjamin Kalas, Thomas Defforge, Gaël Gautier, Arnaud Chaix, Miklós Fried, and Péter Petrik: Development of advanced sensing materials and interface structures for in-situ bioellipsometry, Proc. SPIE 11972, Label-free Biomedical Imaging and Sensing (LBIS) 2022, 119720G (2 March 2022); IF.: 0.38, Conference proceedings

D., Olasz. ; V., Kis ; P., Petrik ; B., Kalas ; G., Sáfrán: Microstructure of composition spread YTiO thin films, In: Miklós Fried (ed.) Proceedings of Symposium on Materials Science, Mátraháza, Magyarország : Óbudai Egyetem (2022) pp. 29-30., 2022 Conference proceedings

Erzsébet Dodony, Aleksander Rečnik, István Dódony, György Sáfrán: In situ TEM study of Ni-silicides formation up to 973K, Journal of Alloys and Compounds Volume 918, 15 October 2022, 165466, Article in periodical IF.: 6.371

Fried, Miklos ; Bogar, Renato ; Takacs, Daniel ; Labadi, Zoltan ; Horvath, Zsolt Endre ; Zolnai, Zsolt: Investigation of Combinatorial WO3-MoO3 Mixed Layers by Spectroscopic Ellipsometry using Different Optical Models, Nanomaterials 2022, 12(14), 2421, Article in periodical IF.: 5.719

Kalas, Benjamin ; Sáfrán, György ; Serényi, Miklós ; Ferencz, Kárpát ; Fried, Miklós ; Petrik, Péter: Surface-enhanced Kretschmann-Raether ellipsometry based on plasmonic, Bragg and waveguide structures,, In: Miklós Fried (ed.) Proceedings of Symposium on Materials Science, Mátraháza, Magyarország : Óbudai Egyetem (2022) pp. 12-14., Conference proceedings

Lohner, Tivadar ; Németh, Attila ; Zolnai, Zsolt ; Kalas, Benjamin ; Romanenko, Alekszej ; Khánh, Nguyen Quoc ; Szilágyi, Edit ; Kótai, Endre ; Agócs, Emil ; Tóth, Zsolt , Judit Budai, Péter Petrik, Miklós Fried, István Bársony, József Gyulai: Disorder and cavity evolution in single-crystalline Ge during implantation of Sb ions monitored in-situ by spectroscopic ellipsometry, Materials Science in Semiconductor Processing Volume 152, December 2022, 107062, Article in periodical IF.: 4.644

Nikolett Hegedüs , Csaba Balázsi , Tamás Kolonits , Dániel Olasz, György Sáfrán , Miklós Serényi , and Katalin Balázsi: Investigation of the RF sputtering process and the properties of deposited silicon oxynitride layers under varying reactive gas conditions, Materials 2022, 15(18), 6313, Article in periodical IF.: 3.748

Nikolett Hegedüs, Riku Lovics, Miklós Serényi, Zsolt Zolnai, Péter Petrik, Csaba Balázsi, Katalin Balázsi: Interpretation of hydrogen incorporation into radio frequency sputtered amorphous silicon based on Berg modelling, Vacuum, Volume 202, August 2022, 111164, Article in periodical IF.: 4.110

Petrik, Peter ; Fried, Miklos: Mapping and imaging of thin films on large surfaces, PHYSICA STATUS SOLIDI A-APPLICATIONS AND MATERIALS SCIENCE, Volume 219, Issue 13, Article Number 2100800, Article in periodical IF.: 2.170.

Budapest, 2022 Szeptember Dr Miklós Fried (PI)